Numerical Simulation Analysis on the Stress and Strain Behavior of Composite Geomembrane in Rigid Landfill

Ming Huang, Teng Tu, Yueling Jing and Fan Yang*

School of Civil and Hydraulic Engineering, Hefei University of Technology, Hefei, 230009, China

INFORMATION

Keywords:
Composite geomembrane
rigid landfill
the finite element method
different working conditions
stress-strain

DOI: 10.23967/j.rimni.2025.10.65484

SCIPEDIA Revista Internacional de Métodos Numéricos para Cálculo y Diseño en Ingeniería

Revista Internacional Métodos numéricos para cálculo y diseño en ingeniería RIMNI CIMNE

Numerical Simulation Analysis on the Stress and Strain Behavior of Composite Geomembrane in Rigid Landfill

Ming Huang, Teng Tu, Yueling Jing and Fan Yang*

School of Civil and Hydraulic Engineering, Hefei University of Technology, Hefei, 230009, China

ABSTRACT

In order to investigate the stress characteristics of a composite geomembrane during the operation of a rigid landfill, a three-dimensional finite element model was developed for a specific rigid landfill project in Tongling China. This model takes into account the contact behavior between the composite geomembrane and concrete unit pool. It aims to calculate and analyze the distribution of stress and strain in both the composite geomembrane and rigid landfill under various working conditions, including empty and full storage. At the same time, the influence of the change of friction coefficient between the composite geomembrane and the concrete cell pool on the stress and strain of the geomembrane is analyzed under the condition of full reservoir. The results indicate that the stress and displacement distribution of the composite geomembrane and concrete structures in the landfill site remain reasonable and safe before and after transitioning from empty to full storage. Under critical conditions, specifically when the cell pool is fully loaded, significant tensile stress and strain occur at the top anchorage of the pool, the edge of the pool bottom, and the corners of the cell pool. The tensile stress in the concrete structure is notably higher at the junction between the side walls and the bottom floor of the cell pool, while compressive stress is more pronounced at the connection between the frame columns of the lower maintenance layer and the bottom floor of the cell pool. Increasing the friction between the composite geomembrane and the concrete cell pool can effectively mitigate stress concentration in the composite geomembrane, thereby enhancing the structural stability and safety.

OPEN ACCESS

Received: 14/03/2025

Accepted: 21/05/2025

Published: 22/09/2025

DOI
10.23967/j.rimni.2025.10.65484

Keywords:
Composite geomembrane
rigid landfill
the finite element method
different working conditions
stress-strain

1 Introduction

In recent years, due to the growth of the economy and the rapid pace of urban development, the generation and disposal of industrial hazardous waste has emerged as a pressing issue [1], with improper disposal posing significant threats to both the ecological environment and human health. The current methods for treating and disposing of hazardous waste primarily encompass incineration, secure land filling, comprehensive utilization of physical and chemical resources, among

*Correspondence: Fan Yang (fyang@hfut.edu.cn).

others [2]. The safe landfill method, among various waste disposal methods, offers the advantages of a straightforward process, flexible and convenient operation, as well as maximum isolation from the natural environment of the biosphere. Consequently, it has gained widespread utilization [3]. The rigid landfill is a reinforced concrete structure specially used for the treatment of hazardous waste, and composite geomembrane usually serves as an important part of its structural anti-seepage system [4]. Due to its characteristics such as lower requirements for geological conditions of the construction site, and fewer requirements for waste indicators entering the site, the rigid landfill is currently in a stage of rapid development [5].

Geosynthetics are synthetic polymer materials, such as plastics and elastomers, that are utilized in civil engineering, hydraulic engineering, and other projects to perform functions including drainage, filtration, seepage prevention, and reinforcement [6]. Geomembrane, as a category of geosynthetic materials, is a flexible and impermeable film manufactured from synthetic materials through specialized processing techniques. And the composite geomembrane is constructed by integrating geomembrane with geotextiles and other multi-layered materials [7]. As an innovative impermeable, the composite geomembrane has gained increasing popularity in water conservancy, municipal, transportation, construction and other projects due to its exceptional impermeability performance and remarkable adaptability to deformation [8–10]. The selection of composite geomembrane as a lining material in the reservoir cell pool of rigid landfill projects is often preferred to effectively mitigate the risk of hazardous waste leakage.

In recent years, the research on the mechanical characteristics of composite geomembranes during operation has focused on earth-rock dams, reservoirs, embankments, and other similar projects. Liu et al. [11] adopted the developed Duncan-Chang model to establish a three-dimensional numerical calculation model of the composite geomembrane core rockfill dam, and analyzed the stress-strain distribution laws of the dam body and the composite geomembrane under the conditions of the completion period and the water storage period. Zhao et al. [12] utilized the finite element method to develop a three-dimensional computational model of a stone-filled dam equipped with a composite geomembrane for seepage prevention. They further analyzed the stress and deformation characteristics of both the dam body and the composite geomembrane on the dam surface before and after water storage. Zhou et al. [13] established a three-dimensional nonlinear finite element model to simulate the construction filling and water storage process, and analyzed the deformation stress of the dam body, the backfill at the bottom of the reservoir and the geomembrane during the water storage period. Koerner et al. [14] calculated the tensile stress of composite geomembrane by using the limit equilibrium method on the basis of assuming that the upper and lower interfaces of composite geomembrane were in the ultimate strength state. Eldesouky et al. [15] conducted a numerical simulation analysis to investigate the local stress-strain behavior of high-density polyethylene geomembranes, and successfully derived its corresponding local stress-strain relationship. Gilbert et al. [16] used the finite element method to study the stress-strain law of composite geomembrane under superimposed loads. Currently, there is a limited amount of research on the utilization of composite geomembrane for rigid landfill seepage prevention both domestically and internationally. During the operation of a rigid landfill, the composite geomembrane is subjected to complex loads, which necessitates research on its stress-strain characteristics to ensure project safety and prevent potential leakage of harmful substances that could compromise both the integrity of the landfill structure and its surrounding environment.

Based on a rigid landfill project in Tongling, this paper develops a finite element model of a rigid landfill site incorporating a composite geomembrane using the finite element software ANSYS. The study analyzes the composite geomembrane within the landfill structure and unit pool under varying

operational conditions, specifically empty and full reservoir scenarios, to determine its stress and strain characteristics along with their variation patterns. Additionally, the influence of the friction coefficient between the composite geomembrane and concrete cell pool on the stress and strain of the geomembrane is evaluated, providing valuable insights for similar projects.

2 The Project Overview

The reservoir area of the rigid landfill engineering at Tongling Solid Waste Treatment Center measures approximately 20,000 m^2, boasting a total storage capacity of around 75,000 m^3. The rigid landfill is compartmentalized into 15 discrete units, with structural expansion joints placed between adjacent units. Each unit comprises 20 individual landfill cell pools, resulting in a total of 300 cell pools across the entire facility.

The principal project of rigid landfill site is designed as an overhead reinforced concrete containment structure, according to the functional requirements, the landfill site is divided into three levels from bottom to top, namely the inspection mezzanine, the reservoir pool body, and the landfill operation layer. The concrete grades of the engineering beams, slabs, columns, and walls are all C35.

The inspection mezzanine consists of a superimposed layer supported by structural columns and shear walls, the clear height of the mezzanine is 2.3 m, specifically designed to meet the requirement of visual detection for potential leakage.

The reservoir pool body is a hazardous waste landfill zone, consisting of 300 landfill cells. The landfill cell pool is a cuboid structure. The net dimensions of each cell pool are 7.05 m × 7.05 m × 5.6 m (length × width × height). The side walls and bottom plate of the reservoir body have a thickness of 0.4 m. Since adjacent landfill unit pools share side-wall retaining walls, the side-wall retaining walls in the storage pool body are designed as bidirectional force-bearing plates.

The mobile rain shelter and traveling crane are installed in the operational layer of the landfill. The mobile rain shelter is to prevent rainwater from entering the repository during the landfill of hazardous waste, and the traveling crane is used for lifting and landfilling hazardous waste.

In addition to utilizing the self-seepage prevention function of concrete, this project also lays composite geomembrane anti-seepage materials. The composite geomembrane is laid on the bottom plate and side walls of the landfill unit pool. It adopts a three-layer integrated structure of "geotextile-geomembrane-geotextile", Specifically, it consists of two layers of non-woven geotextiles with a weight of 600 g/m^2 on the upper and lower sides, and a layer of HDPE geomembrane with a thickness of 2 mm in the middle. To ensure the complete fit between the composite geomembrane and the rigid pool body, the composite geomembrane is fixed at the top of the pool wall with galvanized iron sheets and compacted at the corners of the pool bottom with pressing plates.

3 The Research Methodology

3.1 Constitutive Model for Materials

The rigid landfill concrete materials are considered to be linear elastic substances [17,18] and conform to the generalized Hooke's law of uniform isotropic bodies, with their constitutive equation expressed as follows:

$$\sigma_{ij} = \frac{E}{1+\nu}\varepsilon_{ij} + \frac{\nu E}{(1+\nu)(1-2\nu)}\varepsilon_{kk}\delta_{ij}$$
$$\delta_{ij} = \begin{cases} 1 & i = j \\ 0 & i \neq j \end{cases} \tag{1}$$

where σ_{ij} is the stress tensor; $\varepsilon_{ij}, \varepsilon_{kk}$ are the strain tensor; ν is the Poisson's ratio; E is the modulus of elasticity; δ_{ij} is the kronecker delta.

The foundation soil material is modeled using an ideal elastic-plastic model, which adheres to the Drucker-Prager yield criterion [19]. The expression of this model is as follows:

$$f = \alpha I_1 + \sqrt{J_2} + m = 0 \tag{2}$$

where f is the plastic potential function; I_1 is the first invariant of principal stress; J_2 is the second invariant of deviational stress; α, m are the constants of material, the value of the aforementioned parameter is directly influenced by both the cohesive force exhibited by the material and its internal friction angle.

3.2 Simulation Methodology for Composite GEOMEMBRANE Materials

The composite geomembrane is a flexible material exhibiting excellent tensile properties. The stress-strain relationship of the composite geomembrane during the stress process can be described as follows [20]:

$$T = J(\varepsilon)\,\varepsilon \tag{3}$$

where ε is the tensile strain of the composite geomembrane; T is the tensile stress of composite geomembrane; $J(\varepsilon)$ is the tensile modulus of the composite geomembrane.

The stress-strain curve of the composite geomembrane is presented in Fig. 1, illustrating the ultimate tensile stress (T_{max}) and ultimate tensile strain (ε_{max}), which represent the maximum strength and elongation capacity of the composite geomembrane, respectively. Additionally, T_1 and ε_1 denote the actual working tensile stress experienced by the composite geomembrane.

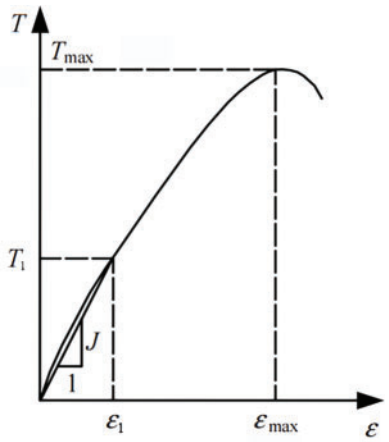

Figure 1: The stress-strain curve of composite geomembrane

The thickness of the composite geomembrane is significantly smaller than the dimensions of the cell pool, posing a challenge for simulation using solid units. Therefore, shell units with a specified

thickness are employed for simulation purposes. In the process of engineering design, it is imperative to maintain a relatively low stress state for the composite geomembrane. As illustrated in Fig. 1, the stress deformation of the composite geomembrane demonstrates linearity during its elastic stage, thereby enabling the application of a linear elastic constitutive model for simulating its behavior [21,22].

3.3 The Method for Simulating the Contact Interface

The material characteristics of composite geomembrane and concrete differ significantly. During the hazardous waste landfill process, there is noticeable friction behavior at the interface between the composite geomembrane and concrete in the cell pool. Therefore, it is essential to consider their contact in order to simulate this frictional shear effect [23]. The surface-to-surface contact model is utilized to simulate the interaction between a composite geomembrane and a concrete cell pool. The contact algorithm in the calculation is implemented by assigning a contact stiffness (spring) using the penalty function method [24]. The penalty function method incorporates a contact spring to establish the relationship between the composite geomembrane and the concrete cell pool. This spring remains inactive when there is separation between the two, but becomes active upon contact closure. The stiffness of this spring, also known as the penalty parameter, determines their contact behavior.

The contact spring undergoes deformation and satisfies the equation under applied load:

$$F = k\Delta \tag{4}$$

where F is the contact force; k is the stiffness of the spring contact; Δ is the degree of interference between contacting surfaces.

4 The Finite Element Computational Model

4.1 Model Establishment and Unit Division

In order to ensure the overall structural stability, deliberate introduction of structural cracks is implemented between every 20 cell pools. This study establishes a three-dimensional finite element model incorporating 20 landfill cell pools, each containing a composite geomembrane, and the underlying foundation. The model adopts a Cartesian coordinate system with the coordinate directions illustrated in Fig. 2. The total height of the rigid landfill is 8.3 m. To mitigate the influence of boundary constraints on the calculation outcomes, an extension measuring 25 m in length and 15 m in depth has been implemented along both the anterior and posterior sides of the landfill (including a 10 m pile foundation within).The Solid65 unit was employed to model the reinforced concrete material and foundation soil, while shell elements were utilized to model the composite geomembrane. The contact element Contact173 and the target element Target170 are employed to simulate the interaction between the concrete cell pool and the composite geomembrane. Upon contact of these two surfaces, contact constraints are established between the contacting surface and the targeted surface, effectively capturing nonlinear tension phenomena.

A fixed constraint is applied to the base surface of the foundation in the calculation. Normal constraints are applied to the front, back, left, and right sides of the foundation. At the same time, according to the anchorage situation of the anti-seepage system mentioned in the project overview, fixed constraints are applied to the anchorage positions of the composite geomembrane.

The entire model is divided into 514,142 units and consists of 523,534 nodes.

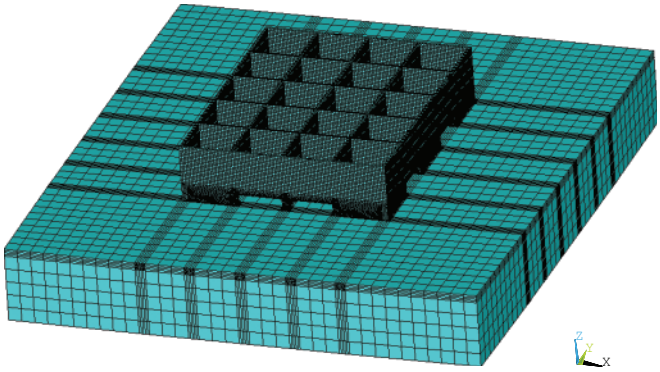

(a) The finite element calculation model of rigid landfill

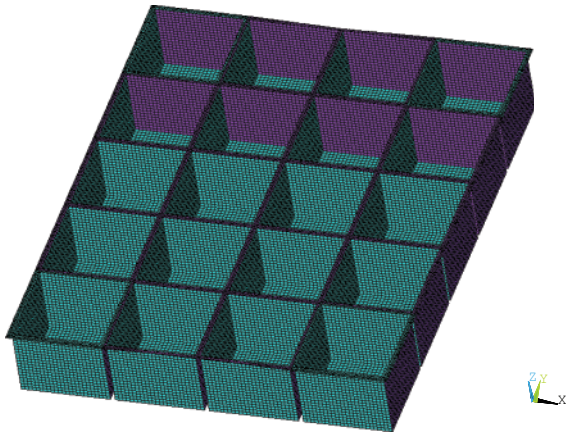

(b) The finite element calculation model of composite geomembrane

Figure 2: The finite element calculation model (a, b)

4.2 The Parameters of Finite Element Calculation

The material parameters of the finite element model were obtained based on relevant literature and project engineering data [25–27], as presented in Table 1.

Table 1: Material parameters calculated by finite element method

Material type	Unit weight (kN/m^3)	Modulus of elasticity (MPa)	Poisson's ratio	Angle of internal friction (°)	Cohesion (kPa)
C35concrete	25	3.25×10^4	0.2	–	–
HDPE composite geomembrane	9.5	1.08×10^3	0.42	–	–

(Continued)

Table 1 (continued)

Material type	Unit weight (kN/m^3)	Modulus of elasticity (MPa)	Poisson's ratio	Angle of internal friction (°)	Cohesion (kPa)
Fully weathered calcareous shale	20	12	0.22	22	30
Highly weathered calcareous shale	22	20	0.3	24	50
Weathered limestone with shale in weak to medium permeable water	24	22	0.32	28	250
Weathered limestone intermingled with shale in slightly permeable water	24	23	0.32	30	500

Coulomb friction is employed to model the contact friction behavior between the composite geomembrane and the concrete cell pool. Based on relevant experimental data and engineering experience [28], the friction coefficient for this interface is established at 0.3.

5 The Analysis of Calculation Results

The study employs a convention whereby tensile stress is represented as positive, compressive stress as negative, and displacement as positive in the upward direction to ensure consistency with established conventions in the field of mechanics.

5.1 Working Condition 1: The Empty Storage of the Cell Pool

The rigid landfill has recently been constructed under these circumstances, with the composite geomembrane being installed, and the current consideration only involves self-weight load.

5.1.1 The Analysis Results of Landfill Structure Calculation

The distribution of the first principal stress and the third principal stress in a rigid landfill is illustrated in Fig. 3. It can be seen from the calculation results that the joint of the side wall and bottom plate of the cell pool will produce a large tensile stress, and the maximum tensile stress value is 0.43 MPa; The maintenance layer of the lower part of the landfill, which includes the frame column and shear wall, will experience significant compressive stress. The maximum compressive stress recorded is 2.17 MPa, observed at the junction between the central frame column and the bottom plate of the landfill site. The stress distribution of a rigid landfill is uniformly distributed.

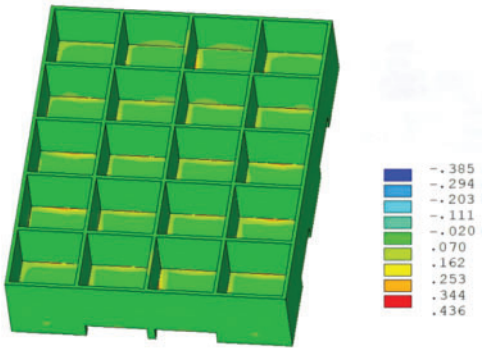

(a) The first principal stress

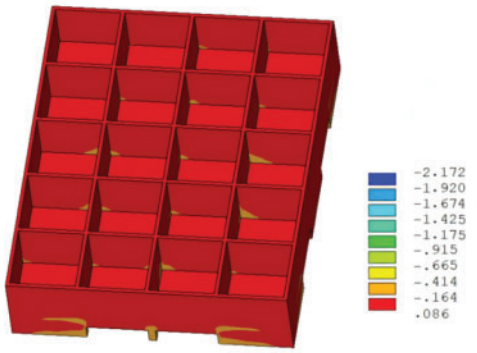

(b) The third principal stress

Figure 3: The main stress cloud map of landfill under working condition 1 (a, b) (unit: MPa)

The vertical displacement distribution of the rigid landfill is illustrated in Fig. 4. The displacement distribution of the entire structure exhibits symmetry. The vertical displacement at the central region of the unit pool is greater compared to that at the periphery, with a maximum value of 0.22 cm observed in the middle section of the unit pool bottom plate near the landfill site's center. The vertical displacement of the base plate in a single cell pool is significant, with the displacement being greater towards the center of the base plate. However, the displacement of the bottom frame column and side wall is minimal.

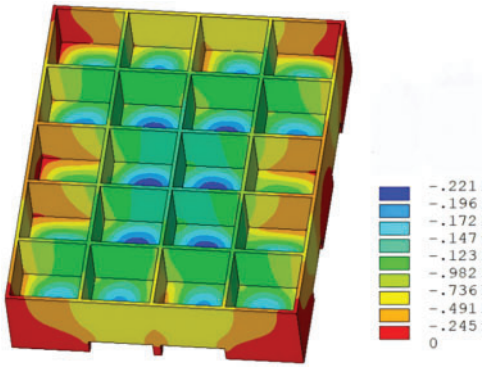

Figure 4: The vertical displacement cloud map of landfill under working condition 1 (unit: cm)

5.1.2 The Analysis Results of Landfill Geomembrane Calculation

According to the calculation results, the stress, strain, and displacement distribution of the composite geomembrane on all four side walls of the cell pool exhibit remarkable similarity. Consequently, one side wall is chosen as a representative for further analysis. The stress, strain, and displacement distribution of the composite geomembrane on the side wall and bottom plate of the cell pool are illustrated in Figs. 5–7.

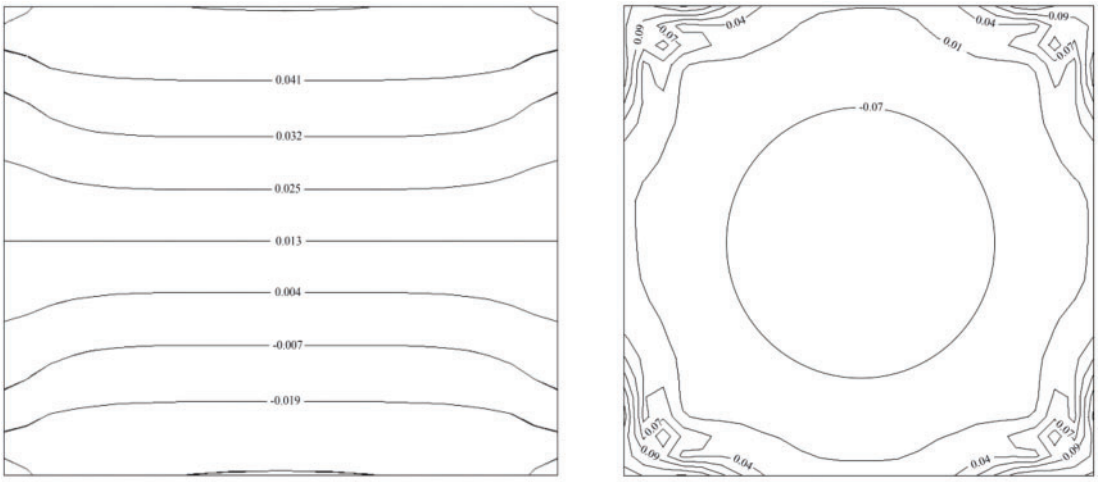

(a) The side wall of the cell pool (b) The base plate of the cell pool

Figure 5: The contour map of the first principal stress in a composite geomembrane under working conditions 1 (a, b) (unit: MPa)

(a) The side wall of the cell pool (b) The base plate of the cell pool

Figure 6: The contour map of the first principal strain in a composite geomembrane under working conditions 1 (a, b) (unit: %)

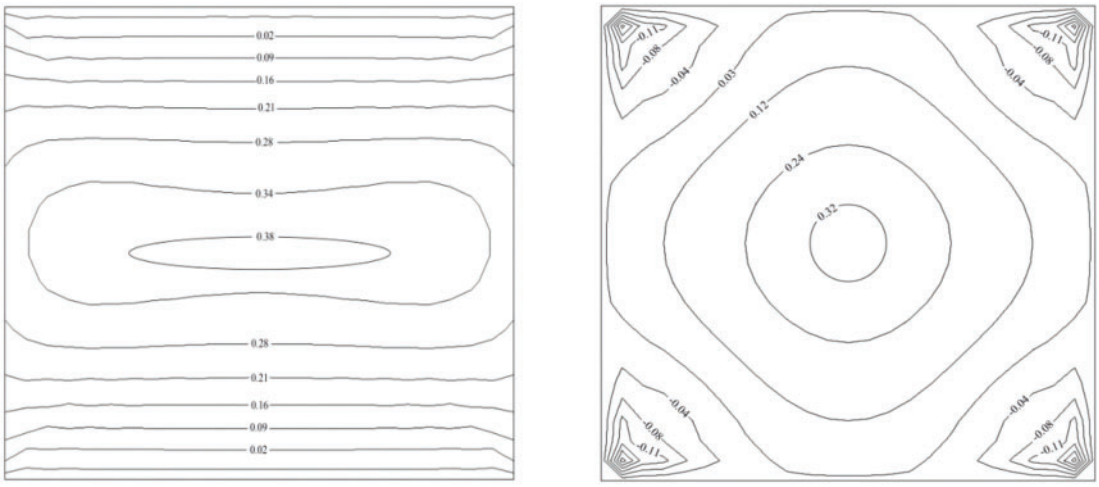

(a) The side wall of the cell pool (b) The base plate of the cell pool

Figure 7: The contour map of the vertical displacement in a composite geomembrane under working conditions 1 (a, b) (unit: cm)

It can be seen from Figs. 5 and 6 that under this working condition, the stress and strain are approximately symmetrical for the sidewall composite geomembrane. Due to the boundary constraint effect, the composite geomembrane surrounding the anchoring of the pool top experiences significant tensile stress and strain. The maximum tensile stress reaches 0.05 MPa, while the maximum tensile strain is 0.19%. As the height of the side wall of the cell pool decreases, there is a gradual reduction in tensile stress. Furthermore, at the lower end of the side wall, a certain compressive stress is exerted on the composite geomembrane. The stress and strain of the composite geomembrane applied to the base plate of the cell pool exhibit approximate central symmetry. At the four corners of the pool's bottom, higher tensile stress and strain are experienced by the composite geomembrane, reaching a maximum tensile stress of 0.09 MPa and a maximum tensile strain of 0.25%. Moving towards the center of the bottom, there is a gradual decrease in tensile stress. Additionally, there is an occurrence of compressive stress acting on the geomembrane.

The maximum vertical displacement of the composite geomembrane on the side wall is illustrated in Fig. 7, exhibiting a slight downward trend at the midpoint of the pool wall with a peak value of 0.38 cm. The proximity to the anchoring area leads to a reduction in vertical displacement. The composite geomembrane exhibits a maximum vertical displacement of 0.26 cm at the base of the cell pool, precisely located at its central bottom. Conversely, minimal vertical displacement is observed at the periphery of the pool bottom.

It can be seen from the results that the stress displacement of both the concrete structure and composite geomembrane during the empty storage period is minimal and uniformly distributed.

5.2 Working Condition 2: The Full Storage of the Cell Pool

Under this condition, the hazardous waste in the rigid landfill cell pool has been filled, and the load considered in this scenario encompasses both self-weight load and hazardous waste load. Since most of the materials landfill in this project are waste salts, taking waste salts as an example, hazardous waste bulk density γ is calculated as 18 kN/m^3.

5.2.1 The Analysis Results of Landfill Structure Calculation

It can be seen from the computed cloud image that the stress and displacement distribution patterns in working condition 2 are similar to those in working condition 1. However, due to the presence of hazardous waste, the stress and displacement values are significantly higher compared to an empty cell pool scenario (Figs. 8 and 9).

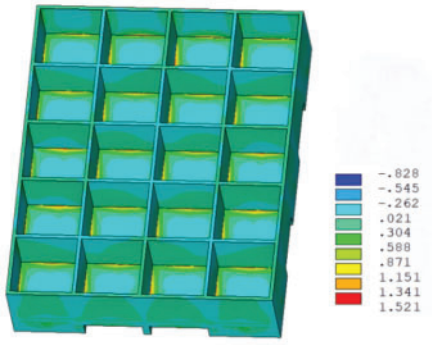

(a) The first principal stress

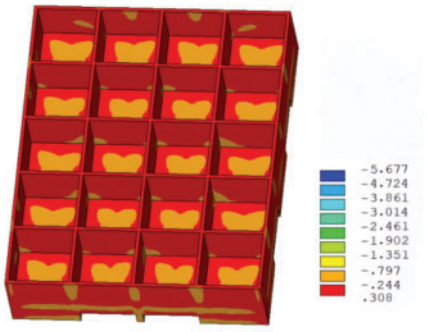

(b) The third principal stress

Figure 8: The main stress cloud map of landfill under working condition 2 (a, b) (unit: MPa)

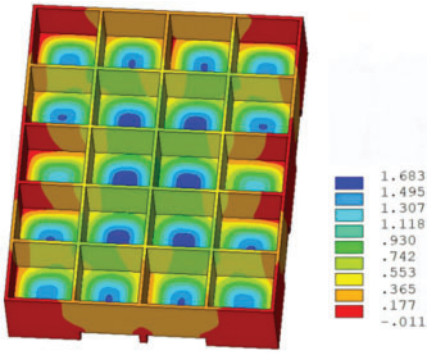

Figure 9: The vertical displacement cloud map of landfill under working condition 2 (unit: cm)

The distribution of the first principal stress and the third principal stress of the rigid landfill site when all cell pools are full is illustrated in Fig. 8. In this scenario, a significant tensile stress occurs at the corner where the bottom plate of the cell pool meets the side wall, with a maximum value of 1.52 MPa. Additionally, there is a maximum compressive stress of 5.68 MPa observed. Consequently, substantial vertical displacement can be expected at the center of the base plate for each unit pool, reaching a maximum magnitude of 1.68 cm.

5.2.2 The Analysis Results of Landfill Geomembrane Calculation

It can be seen from Figs. 10 and 11 that under the specified operational conditions, the composite geomembrane installed on the side wall of the cell pool experiences a maximum tensile stress of 0.74 MPa, with a corresponding maximum tensile strain of 2.68%. This critical condition is observed near the anchorage point at the top of the cell pool. Additionally, significant tensile stress and strain are also observed at the corner region of the side wall due to hazardous waste influence. Consequently, compressive stress occurs in this composite geomembrane. And as for the composite geomembrane on the base plate of the cell pool, the stress and strain are approximately center-symmetric distribution. Near the edge of the pool bottom, the composite geomembrane experiences higher tensile stress and strain, with a maximum tensile stress of 0.48 MPa and a maximum tensile strain of 2.58%. At the four corners of the pool bottom, compressive stress is generated in the composite geomembrane, with a maximum compressive stress of 0.21 MPa.

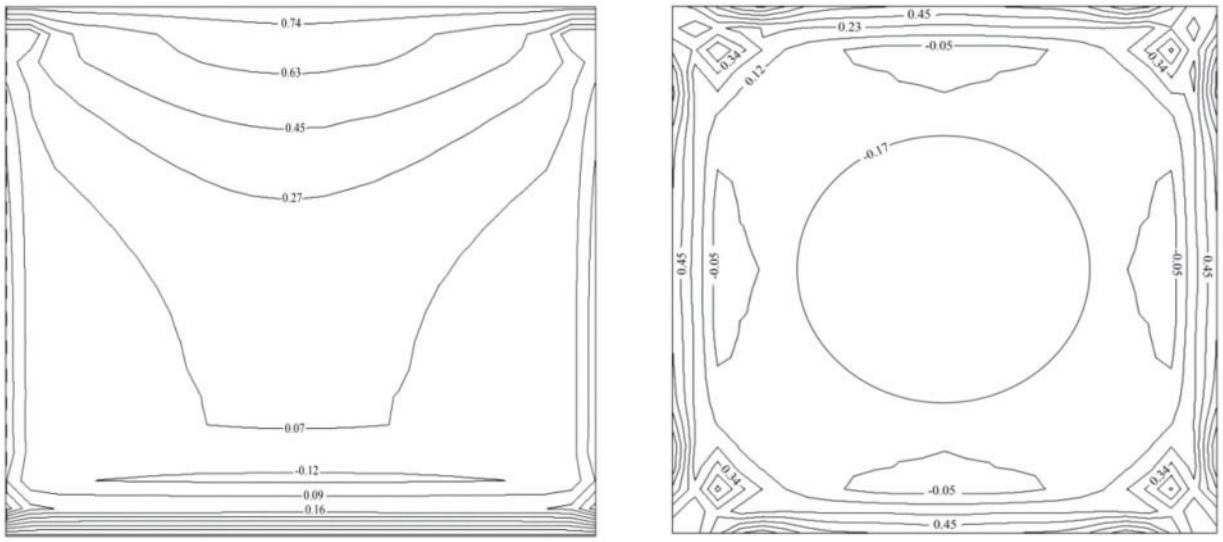

(a) The side wall of the cell pool (b) The base plate of the cell pool

Figure 10: The contour map of the first principal stress in a composite geomembrane under working conditions 2 (a, b) (unit: MPa)

(a) The side wall of the cell pool (b) The base plate of the cell pool

Figure 11: The contour map of the vertical displacement in a composite geomembrane under working conditions 2 (a, b) (unit: %)

The vertical displacement distribution of the composite geomembrane in the cell pool is depicted in Fig. 12. It can be observed from the figure that the maximum downward vertical displacement of the composite geomembrane on the sidewall of the cell pool measures 4.83 cm and occurs at a quarter height position along the sidewall. And the vertical displacement of the composite geomembrane on the bottom of the pool demonstrates approximate central symmetry, with a maximum downward vertical displacement of 1.71 cm observed at the central region. Moving towards the periphery of the pool's bottom, there is a gradual reduction in the magnitude of vertical displacement experienced by the composite geomembrane.

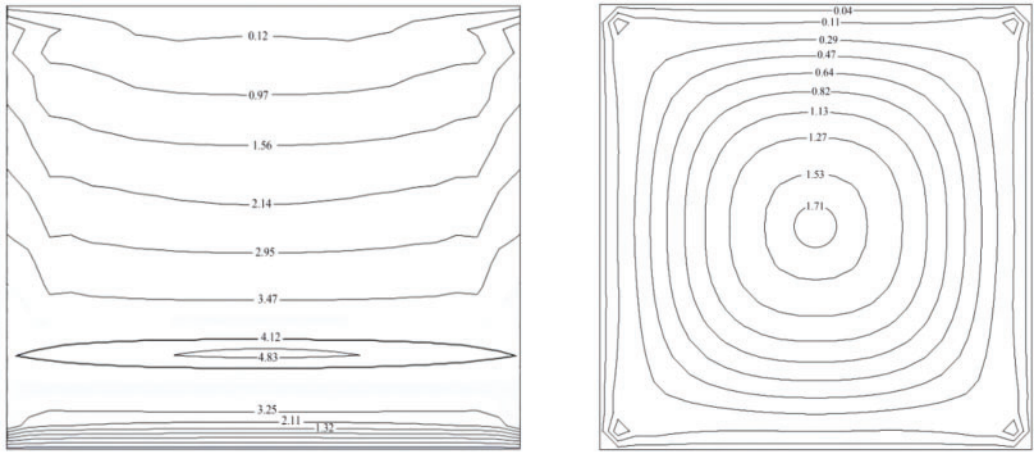

(a) The side wall of the cell pool (b) The base plate of the cell pool

Figure 12: The contour map of the vertical displacement in a composite geomembrane under working conditions 2 (a, b) (unit: cm)

5.3 The Overview of Other Working Conditions and Assessment of Structural Safety

5.3.1 The Overview of Other Working Conditions

The calculations and analyses in Sections 5.1 and 5.2 cover two typical working conditions: the empty storage of the cell pool during the construction and completion period, and the fully-filled storage of the cell pool when the landfill is completed. Meanwhile, this paper also calculates two working conditions in the mid-term of hazardous waste landfill, namely, after filling one cell pool and after filling a row of cell pools, as shown in Fig. 13. The red areas in the figure represent the hazardous waste that has been land filled in the cell pools.

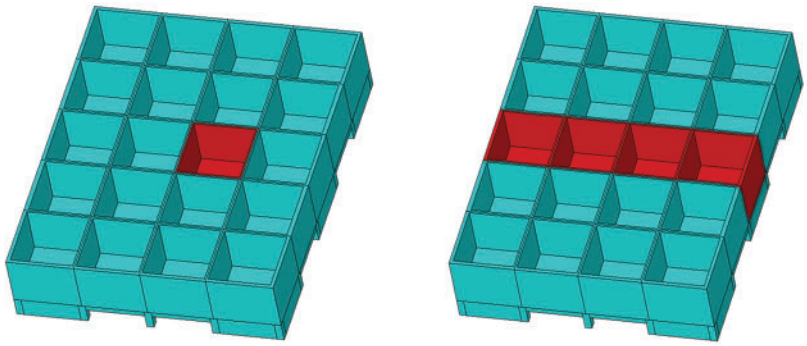

(a) filling one cell pool (b) filling a row of cell pools

Figure 13: Two working conditions in the mid-term of hazardous waste landfill (a, b)

In Fig. 13a, for the cell pool in which hazardous waste has been landfilled, all four side walls are subjected to unidirectional loads, In Fig. 13b, there will also be side walls subject to unilateral forces. Both of these working conditions are hazardous working conditions to the side walls of the cell pools, which are subjected to unidirectional forces. For these unilaterally-stressed side walls, a large tensile stress occurs at the connection part between the lower end of the side wall and the edge of the bottom plate, and significant horizontal displacements will take place in the middle and upper regions of the side wall.

Tables 2 and 3 respectively present the maximum values of stress and displacement of the concrete structure of the rigid landfill under four working conditions, as well as the maximum values of stress, strain and displacement of the composite geomembrane.

Table 2: Finite element calculation results of landfill concrete structures under four working conditions

Conditions	Maximum values of stress (MPa)		Maximum values of displacement (cm)		
	Compressive stress	Tensile stress	*X*-direction	*Y*-direction	*Z*-direction
The empty storage of the cell pool	2.17	0.43	0.05	0.05	0.22

(Continued)

Table 2 (continued)

Conditions	Maximum values of stress (MPa)		Maximum values of displacement (cm)		
	Compressive stress	Tensile stress	*X*-direction	*Y*-direction	*Z*-direction
Filling one cell pool	2.78	0.96	0.41	0.42	0.76
Filling a row of cell pools	4.45	1.21	0.77	0.84	1.35
The full storage of the cell pool	5.68	1.52	0.89	0.92	1.68

Table 3: Finite element calculation results of landfill composite geomembrane under four working conditions

Conditions	Maximum tensile stress (MPa)	Maximum tensile strain (%)	Maximum values of displacement (cm)		
			X-direction	*Y*-direction	*Z*-direction
The empty storage of the cell pool	0.09	0.25	0.02	0.06	0.38
Filling one cell pool	0.54	2.15	0.05	0.09	3.16
Filling a row of cell pools	0.65	2.34	0.06	0.12	3.63
The full storage of the cell pool	0.74	2.68	0.12	0.23	4.83

5.3.2 The Assessment of Structural Safety

The stress safety factor K_T and strain safety factor K_ε of the composite geomembrane are derived from the following equation [20].

$$\begin{cases} K_T = T_{\max}/T_1 \\ K_\varepsilon = \varepsilon_{\max}/\varepsilon_1 \end{cases} \tag{5}$$

According to the specifications and relevant literature [29–31], when the stress-strain level of a composite geomembrane is limited to less than 20%, its service life will be significantly extended. Therefore, a safety factor K of 5 has been selected in this study, and when K_T and K_ε are greater than 5, it indicates that the composite geomembrane is in a safe condition.

The calculation results indicate that under the full reservoir condition (i.e., the most unfavorable working condition), the side wall composite geomembrane experiences a maximum tensile stress of 0.74 MPa and a maximum tensile strain of 2.68%, while the pool bottom composite geomembrane experiences a maximum tensile stress of 0.48 MPa and a maximum tensile strain of 2.58%.

According to the material parameters of the composite geomembrane utilized in this project, it exhibits an ultimate tensile strength of 20 MPa and an ultimate yield elongation of 15%. The calculated stress safety factor (K_T) is determined to be 27, while the strain safety factor (K_ε) measures at 5.6, both meeting the requirement for a safety factor greater than 5.The use of composite geomembrane for seepage prevention in rigid landfills demonstrates a significant safety margin.

At the same time, the maximum tensile stress and compressive stress experienced by the concrete structure in the rigid landfill site are 1.52 and 5.67 MPa, respectively, which are below the specified design values for tensile and compressive strength of C35 concrete as stated in code [26].

5.4 Influence of Different Friction Coefficients on Stress-Strain of Composite Geomembrane

This section focuses on analyzing the impact of the friction coefficient (μ) on the stress-strain behavior of composite geomembranes in a fully filled cell pool scenario. By maintaining all other computational conditions constant, the stress-strain distribution of the composite geomembrane is evaluated for contact friction coefficients of 0.5 and 0.8. Figs. 14 and 15 illustrate the variation patterns of maximum principal stress and maximum principal strain for the composite geomembrane when μ equals 0.5. Additionally, Figs. 16 and 17 depict the distribution patterns of stress and strain for the composite geomembrane when μ equals 0.8.

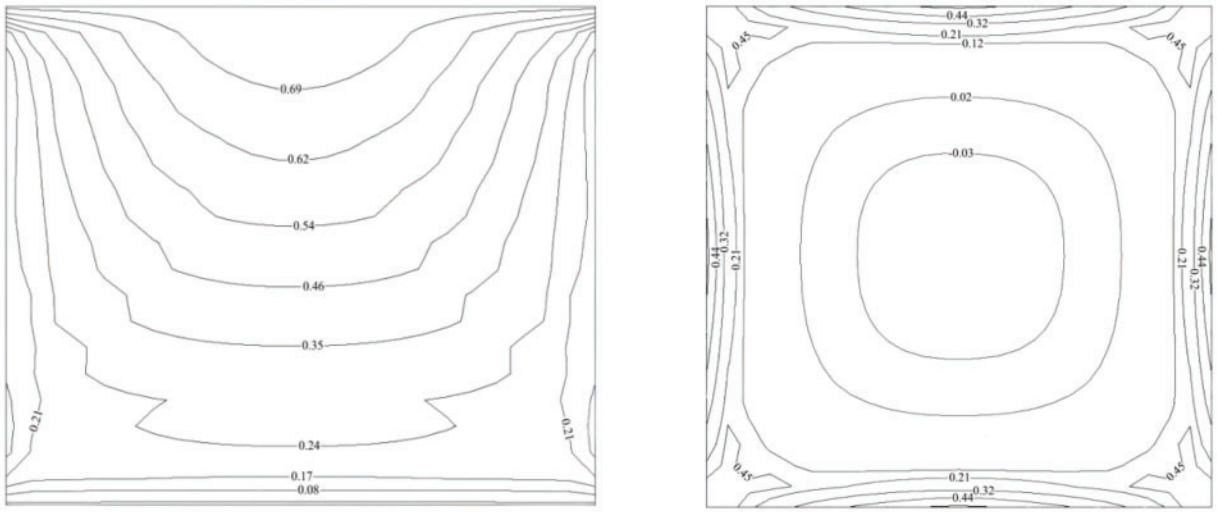

(a) The side wall of the cell pool

(b) The base plate of the cell pool

Figure 14: The contour map of the first principal stress in a composite geomembrane when the friction coefficient is 0.5 (a, b) (unit: MPa)

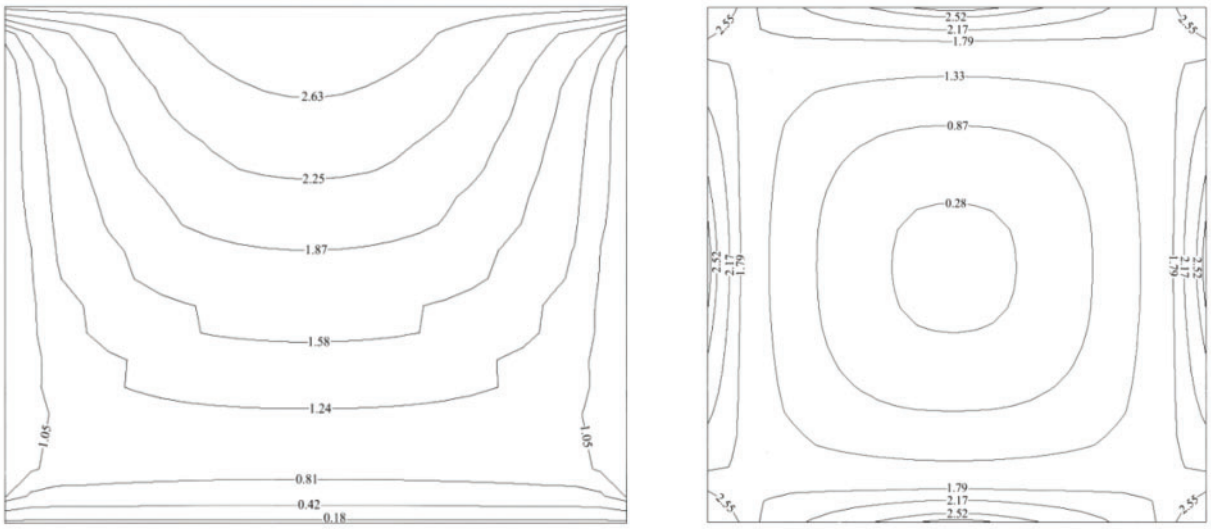

(a) The side wall of the cell pool (b) The base plate of the cell pool

Figure 15: The contour map of the first principal strain in a composite geomembrane when the friction coefficient is 0.5 (a, b) (unit: %)

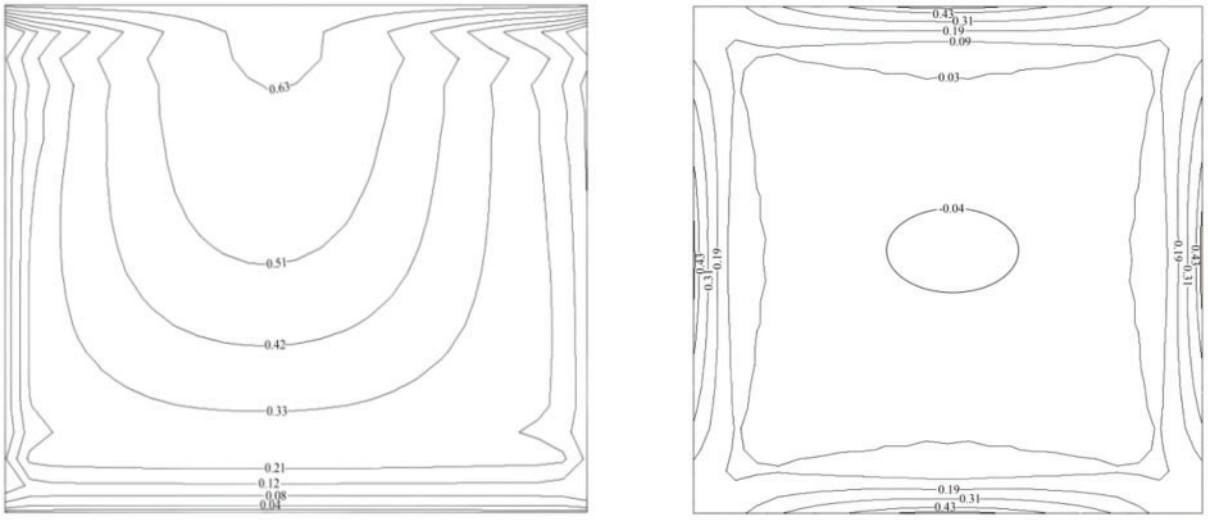

(a) The side wall of the cell pool (b) The base plate of the cell pool

Figure 16: The contour map of the first principal stress in a composite geomembrane when the friction coefficient is 0.8 (a, b) (unit: MPa)

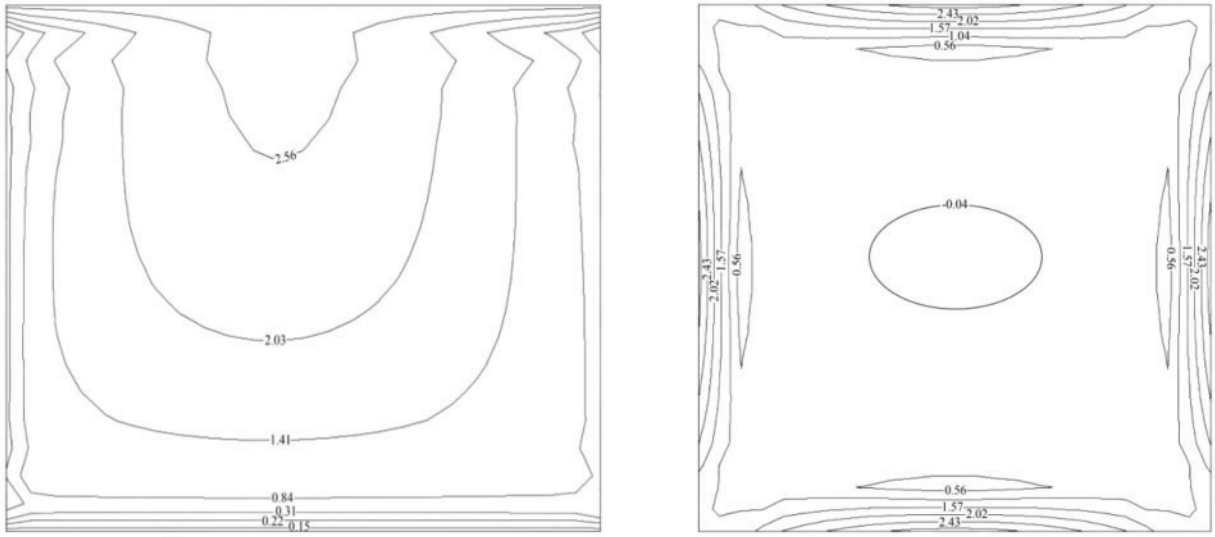

(a) The side wall of the cell pool (b) The base plate of the cell pool

Figure 17: The contour map of the first principal strain in a composite geomembrane when the friction coefficient is 0.8 (a, b) (unit: %)

It can be seen from the figure that the change of the contact friction coefficient between the composite geomembrane and the concrete unit pool has a certain influence on the stress deformation of the composite geomembrane. The results indicate that both the maximum tensile stress and strain of the composite geomembrane exhibit a decreasing trend as the contact friction coefficient increases. Specifically, when the contact friction coefficient increases from 0.3 to 0.8, the maximum tensile stress of the composite geomembrane decreases from 0.74 to 0.63 Mpa. The maximum tensile strain decreases from 2.68% to 2.56%. The maximum tensile stress of composite geomembrane decreases from 0.48 to 0.43 Mpa, and the maximum tensile strain decreases from 2.68% to 2.51%. Furthermore, the stress-strain contour map illustrates that increasing the contact friction coefficient effectively diminishes the area of the composite geomembrane subjected to higher tensile stress. Consequently, in engineering applications, appropriately enhancing the friction between the composite geomembrane and the concrete unit pool can mitigate the stress-strain state of the composite geomembrane, thereby improving the structural stability and safety.

6 Conclusion

The finite element method is employed in this study to simulate the rigid landfill with a composite geomembrane. The stress displacement analysis focuses on evaluating the overall structural behavior of the landfill and the composite geomembrane within the cell pool, considering various operational conditions such as empty and full landfills. The obtained results demonstrate that:

The symmetrically designed rigid landfill site analyzed in this paper exhibits approximate symmetry in both stress and displacement of the entire structure as well as the composite geomembrane laid within the cell pool when subjected to symmetrical loads.

When the rigid landfill is empty, the stress displacement of the concrete structure and composite geomembrane is minimal. The stress deformation in most areas of the landfill is nearly uniform, with

only tensile stress generated at the corner of the unit pool. The maximum values for stress and strain in the composite geomembrane occur at its anchorage area.

When the landfill unit pool reaches full capacity, the stress and displacement experienced by the rigid concrete structure of the landfill and the composite geomembrane within the pool significantly increase compared to the empty condition. The maximum tensile stress recorded at the landfill site is 1.52 MPa, occurring at the junction between the side wall and the bottom plate of the cell pool. The maximum vertical displacement is 1.68 cm, observed at the center of the cell pool's bottom plate. Additionally, the connection structure between the independent frame column of the landfill maintenance sandwich and the upper bottom plate experiences substantial compressive stress, with a peak value of 5.68 MPa. The composite geomembrane exhibits significant tensile stress and strain at the top anchorage of the pool, the edge of the bottom of the pool, and the corners of the cell pool, reaching a maximum tensile stress of 0.74 MPa and a maximum tensile strain of 2.68%, both occurring at the top anchorage. Furthermore, compressive stress is generated in most central areas of the side walls and bottom plate of the composite geomembrane. The maximum vertical displacement of the composite geomembrane on the side wall is 4.83 cm, noted at one-quarter height of the side wall of the unit pool, while the maximum vertical displacement on the bottom of the pool is 1.71 cm, located at the center of the pool. Increasing the contact friction coefficient between the composite geomembrane and the concrete cell pool can effectively reduce the tensile stress and strain in the anchoring area, thereby alleviating the overall stress-strain state of the composite geomembrane.

The analysis indicates that the stress and deformation distribution of the composite geomembrane installed in the rigid landfill project, as well as in the cell pool before and after reservoir emptying and filling, remains within a reasonably controllable range. Nevertheless, during both construction and operation phases of the landfill, particular attention should be given to areas with high tensile stress near the geomembrane anchorage zones and at the corners of the cell pool. During the operational lifespan of the landfill, effective monitoring must be implemented to prevent hazardous waste leakage caused by long-term tensile cracking of the composite geomembrane. From a technical perspective, applying an adhesive waterproof coating or utilizing self-adhesive waterproof coils within the cell pool can enhance the integrity of the composite geomembrane placement while increasing the friction coefficient between the geomembrane and the cell pool, thereby reducing stress concentration on the composite geomembrane.

Acknowledgement: The authors would like to express their gratitude for the valuable feedback and suggestions provided by all the anonymous reviewers and the editorial team.

Funding Statement: This work is supported by Anhui Provincial Natural Science Foundation: Water Science Joint Fund (2208085US01, 2308085US01) and Youth Fund (2308085QE194).

Author Contributions: The authors confirm their contribution to the paper as follows: study conception and design: Ming Huang, Teng Tu, Yueling Jing, Fan Yang; data collection: Ming Huang, Teng Tu; analysis and interpretation of results: Ming Huang, Teng Tu, Yueling Jing, Fan Yang; draft manuscript preparation: Ming Huang, Teng Tu. All authors reviewed the results and approved the final version of the manuscript.

Availability of Data and Materials: Data is available upon request.

Ethics Approval: Not applicable.

Conflicts of Interest: The authors declare no conflicts of interest to report regarding the present study.

References

1. Prasad R, Mahmood AK. Hazardous waste in the Asian Pacific region. Rev Environ Health. 2011; 24(1):31–8. doi:10.1515/reveh.2011.005.
2. Stemn E, Kumi-Boateng B. Hazardous waste landfill sites-election in Western Ghana: an integration of multicriteria decision analysis and geographic information system. Waste Manage Res. 2019;37(7):723–36. doi:10.1177/0734242X19854530.
3. Huang CY, Ning SY. The design and application of hazardous waste. Yunnan Chem Technol. 2023;50(9):94–7. (In Chinese). doi:10.3969/j.issn.1004-275X.2023.09.24.
4. Qiu XP, Luo XY, Chen L, Luo X, Wei J, Li XR. Design and economic analysis of rigid landfill for hazardous wast. Environ Sanit Eng. 2020;28(6):80–5. (In Chinese). doi:10.19841/j.cnki.hjwsgc.2020.06.013.
5. Li T, Zhu WP, Liu CH, Zhang H. Brief discussion on the construction status and development of flexible landfills and rigid landfills. J Qinghai Environ. 2022;32(4):190–4. (In Chinese). doi:10.3969/j.issn.1007-2454.2022.04.006.
6. Rowe RK, Jones CJ. Geosynthetics: innovative materials and rational design. In: GeoEng 2000 International Conference on Geotechnical and Geological Engineering; 2000 Nov 19–24; Melbourne, VIC, Australia. p. 1124–56.
7. Rowe RK, Somuah M. Effects of perfluoroalkyl substances (PFAS) on antioxidant depletion from a high-density polyethylene geomembrane. J Environ Manage. 2023;328(6):116979. doi:10.1016/j.jenvman.2022.116979.
8. Wu Y, He JX, Liu L, Yang HH. Testing the shearing creep of composite geomembranes cushion interface and its empirical model. Soils Found. 2023;62:e02212. doi:10.1016/j.sandf.2022.101236.
9. Fernando LL, Marcelo K, Clever A, Maria L, Ennio MP, Jefferson L. Service life of some HDPE geomembranes. Case Stud Constr Mater. 2017;18(6):110–114, 129. doi:10.1016/j.cscm.2023.e02212.
10. Lou B, Cui HY, Liu HY, Yu J. Durability of composite geomembrane in Zhaokou Yellow river irrigation area. Yellow River. 2022;44(11):114–7. (In Chinese). doi:10.3969/j.issn.1000-1379.2022.11.022.
11. Liu SC, Wang K, Xiong J, Wang T. Stress-strain analysis of geomembrane core rockfill dam based on Duncan-Chang model. China Rural Water Hydropower. 2025;(1):215–220, 226. (In Chinese). doi:10.12396/znsd.240184.
12. Zhao YH, Li ZH, Chen SN. Finite-element stress and deformation analysis of a geomembrane face rockfill dam. Pearl River. 2022;43(8):83–7. (In Chinese). doi:10.3969/j.issn.1001-9235.2022.08.013.
13. Zhou YQ, Shen ZZ, Wang W. Deformation and stress behavior analysis of upper reservoir with composite geomembrane as impermeable material. South-to-North Water Transfers Water Sci Technol. 2014;12(2):160–163, 174. (In Chinese). doi:10.13476/j.cnki.nsbdqk.2014.02.038.
14. Koerner RM, Hwu B-L. Stability and tension considerations regarding cover soils on geomembrane lined slopes. Geotext Geomembr. 1991;10(4):335–55. doi:10.1016/0266-1144(91)90010-T.
15. Eldesouky HMG, Brachman RWI. Viscoplastic modelling of HDPE geomembrane local stresses and strains. Geotext Geomembr. 2020;48(1):41–51. doi:10.1016/j.geotexmem.2019.103503.
16. Gilbert RB, Long JH, Daly JJ. Strutural integrity of composite geosyntheticlining and cover systems. Proc Conf Ceosynth. 1993;5(2):1389–401. doi:10.13719/10.1360/zf1993.05.02.
17. Ai Z, Wang S, Zhang L. Static-dynamic three-dimensional finite element reinforcement calculation of Kundulun flood flushing cave structure. Water Resources Hydropower Eng. 2024;55(1):39–43. (In Chinese). doi:10.13928/j.cnki.wrahe.2024.S1.005.
18. Zhen GJ, Li ZH, Ling W. Stress and deformation characteristics of Tongcheba reservoir mudstone slag dam integrated seepage prevention system of composite geomembrane and concrete cut off wall. Water Resources Power. 2024;42(4):147–150, 172. (In Chinese). doi:10.20040/j.cnki.1000-7709.2024.20231002.

19. Zhou FX, Li SR. Generalized Drucker-Prager strength criterion. Rock Soil Mech. 2008;29(3):747–51. (In Chinese). doi:10.16285/j.rsm.2008.03.028.
20. Cen WJ, Shen CS, Tong JW. Study of construction behavior of composite geomembrane rockfill dam on thick alluvium deposit. Rock Soil Mech. 2009;30(1):175–80. (In Chinese). doi:10.3969/j.issn.1000-7598.2009.01.030.
21. Yuan J, Pan WZ, An JJ. Application of composite geomembrane to anti-seepage structure in Yellow River sluice. Yellow River. 2019;41(1):111–5. (In Chinese). doi:10.3969/j.issn.1000-1379.2019.01.025.
22. Huang W, Lei XY, Liu XN, Wang YJ, Zhu S, Sun TJ. Research on connection joint between asphalt concrete slab and geomembrane: case of Jurong pumped storage power station in Jiangsu province. Yangtze River. 2024;55(11):67–73. (In Chinese). doi:10.16232/j.cnki.1001-4179.2024.11.009.
23. Yu JP. Analysis of stress and deformation characteristics of geomembrane protection for hydraulic structures. Shanxi Water Resources. 2022;11(2):50–3. (In Chinese). doi:10.13719/j.cnki.50-53.2022.01.045.
24. Zhang HW, Gao XS, Zhang QY. ANSYS method of nonlinear finite element analysis and its application examples. Beijing, China: China Water & Power Press; 2013.
25. Zhao SG. Adopting finite element method to analyze the material—taking C35 concrete as the example. Heilongjiang Hydraulic Sci Technol. 2018;46(1):1–3, 23. (In Chinese).
26. Ministry of Housing and Urban-Rural Development of the People's Republic of China. Code for design of concrete structures, GB50010-2010. Beijing, China: China Architecture & Building Press; 2010.
27. Ministry of Water Resources of the People's Republic of China. Standard for application of geosynthetic in hydraulic and hydro-power engineering, SL/T225-98. Beijing, China: China Water & Power Press; 1998.
28. Editorial Board for the Engineering Application Handbook of Geosynthetic Materials. Geosynthetic materials engineering a pplication manual. Beijing, China: China Architecture & Building Press; 2000.
29. Yang Y, Liu H, Huang SX. Stress-strain analysis of anti-seepage composite geomembrane of reservoir basin and reservoir bank in karst areas. China Rural Water Hydro-Power. 2021;7(2):146–50. (In Chinese). doi:10.3969/i.issn.1003-3114.2021.07.003.
30. Yin BH. Application practice of composite geomembrane in Xixianyuan anti-regulation reservoir dam. Zhengzhou, China: The Yellow River Water Conservancy Press; 2010.
31. Kong FH, Hua JJ, Wang LH. Stress and deformation analysis of the composite geomembrane used as the seepage prevention for the whole reservoir basin on deep overburden. China Rural Water Hydro-Power. 2018;5(3):152–5. (In Chinese).